

A vascularized three-dimensional model integrating primary breast tumor cells and microvascular fragments: mimicking the tumor microenvironment involved in chemoresistance

Received: 15 September 2025

Accepted: 25 December 2025

Published online: 08 January 2026

Cite this article as: Lo Cicero A., La Monica F., Lo Buglio G. *et al.* A vascularized three-dimensional model integrating primary breast tumor cells and microvascular fragments: mimicking the tumor microenvironment involved in chemoresistance. *Cancer Cell Int* (2025). <https://doi.org/10.1186/s12935-025-04154-6>

Alessandra Lo Cicero, Francesco La Monica, Gabriele Lo Buglio, Simona Campora, Federico Gangemi, Paolo Cinà, Monica Salamone, Margot Lo Pinto, Simone Dario Scilabra & Giulio Gherzi

We are providing an unedited version of this manuscript to give early access to its findings. Before final publication, the manuscript will undergo further editing. Please note there may be errors present which affect the content, and all legal disclaimers apply.

If this paper is publishing under a Transparent Peer Review model then Peer Review reports will publish with the final article.

A Vascularized Three-Dimensional Model Integrating Primary Breast Tumor Cells and Microvascular Fragments: Mimicking the Tumor Microenvironment Involved in Chemoresistance

Alessandra Lo Cicero^{1*}, Francesco La Monica¹, Gabriele Lo Buglio^{1,2}, Simona Campora¹, Federico Gangemi¹, Paolo Cinà³, Monica Salamone⁴, Margot Lo Pinto⁵, Simone Dario Scilabra⁵, Giulio Gherzi^{1,3**}

¹ Department of Biological, Chemical and Pharmaceutical Sciences and Technologies (STEBICEF), University of Palermo, Palermo, Italy

² Department of Pharmacy, University of Copenhagen, Copenhagen, Denmark

³ Abiel srl, Palermo, Italy

⁴ Institute for Biomedical Research and Innovation, National Research Council (IRIB-CNR), Palermo, Italy

⁵ Proteomics Group of Ri.MED Foundation, Research Department IRCCS ISMETT (Istituto Mediterraneo per i Trapianti e Terapie ad Alta Specializzazione), Palermo, Italy

*Corresponding author: Department of Biological, Chemical and Pharmaceutical Sciences and Technologies (STEBICEF), University of Palermo, Viale delle Scienze, Ed. 16 – 90128 Palermo – Italy.

E-mail: alessandra.locicero@unipa.it

**Corresponding author: Department of Biological, Chemical and Pharmaceutical Sciences and Technologies (STEBICEF), University of Palermo, Viale delle Scienze, Ed. 16 – 90128 Palermo – Italy.

E-mail: giulio.ghersi@unipa.it

Abstract

Background

Tumorigenesis is a complex and dynamic process in which the tumor microenvironment (TME) plays a central role. In solid tumors, the TME contributes to key mechanisms of tumor progression, including metastasis, immune evasion, and resistance to therapies. One major challenge in preclinical cancer research is the development of reliable three-dimensional (3D) in vitro models, which more accurately replicate the in vivo tumor architecture and microenvironmental conditions,

such as hypoxia and extracellular matrix (ECM) organization. However, reproducing functional vascular networks and neo-angiogenesis within these models remains a key challenge.

Methods

In this study, an advanced 3D tumor model, referred to as angiotumoroids, was developed by co-culturing primary murine breast tumor cells (PTCs) with species-specific adipose-derived microvascular fragments (MVs). Angiotumoroids were characterized using scanning electron microscopy and immunostaining, and angiogenesis was evaluated through collagen gel sprouting assays. High-resolution proteomic profiling was conducted, focusing on signatures associated with angiogenesis, extracellular matrix (ECM) composition, and tissue remodeling. Additionally, the response and internalization to anticancer drug treatments were evaluated.

Results

MVs are successfully integrated in angiotumoroids, resulting in the formation of vasculature-like structures and demonstrating robust structural organization with dynamic modulation of matrix metalloproteinase 9. Formation of neovasculature was visualized through sprouting and branching, driven by both direct PTC–MV interactions and PTC-conditioned media, highlighting the roles of juxtacrine and paracrine signaling.

Proteomic profiling revealed distinct expression patterns associated with angiogenesis, ECM components (including collagen types I and IV), and active ECM remodeling with elevated MMP expression. Additionally, angiotumoroids showed increased expression of ATP-binding cassette (ABC) transporters, particularly ABCB1 (P-glycoprotein), suggesting potential mechanisms of drug efflux.

Functionally, angiotumoroids demonstrated reduced sensitivity to doxorubicin compared to PTC spheroids, maintaining structural integrity and higher cell viability post-treatment. Time-course analysis revealed preferential doxorubicin accumulation in MVF-enriched regions, as confirmed by colocalization with CD31, indicating a spatially regulated distribution of the drug mediated by the vascular compartment.

Conclusions

Collectively, these findings establish angiotumoroids as a robust and physiologically relevant in vitro model for studying tumor vascularization, ECM dynamics, and therapeutic response. This platform holds significant promise for predictive cancer research and preclinical drug screening, bridging the gap between traditional in vitro systems and in vivo models.

Keywords

Angiogenesis; Spheroids; Microvascular fragments; Tumor microenvironment; 3D tumor model

Background

Solid tumor microenvironment (TME) plays a key role in cancer development, providing a supportive niche for tumor initiation, growth, and expansion. It surrounds tumor cells, supplies essential nutrients and oxygen, modulates tumor cell behavior, establishes an immunosuppressive environment to evade the immune system, and acts as a barrier to effective drug delivery [1,2]. The TME consists of cellular components, such as cancer-associated fibroblasts (CAFs), infiltrating immune cells, endothelial cells, and pericytes from blood vessels, as well as non-cellular components, including the extracellular matrix (ECM) and signaling molecules [3]. Rapid tumor cell proliferation depletes nutrients and oxygen in the early stages of tumor growth, creating a hypoxic environment that inhibits further tumor expansion [4]. In response to hypoxia, the "angiogenic switch" is triggered, reinitiating tumor growth by promoting new vessel formation [5,6]. This process is mediated by hypoxia-inducible factors (HIFs), which are produced under low oxygen conditions and drive tumor progression and angiogenesis by activating pro-angiogenic genes, such as vascular endothelial growth factor (VEGF), platelet-derived growth factor (PDGF), and matrix metalloproteinases (MMP-2 and MMP-9). The interplay of these molecules leads to sprouting angiogenesis, by specialized endothelial cells known as tip cells, which guide the

formation of new vessels from pre-existing blood vessels [5] through MMP-mediated degradation and ECM protein synthesis, establishing stiffness and adhesion gradients [5] [7].

Vascularized regions within solid tumors significantly impact drug uptake and, consequently, the efficacy of chemotherapeutic treatments [8]. The effective delivery of anticancer agents throughout solid tumors is primarily determined by the structural and functional properties of the tumor vasculature, as well as the physicochemical characteristics of the extracellular matrix (ECM), which govern drug transport within the target tissue. Additionally, drug transport through the extravascular compartment occurs via diffusion or convection, with penetration depth often limited by rapid intracellular uptake of the drug by tumor cells near microvascular structures [9].

To gain deeper insights into TME's role and its interactions with cancer cells, significant efforts are being directed toward developing advanced three-dimensional (3D) models that emulate the TME complexity [2]. In recent decades, 3D cell cultures, such as spheroids and organoids, have been developed to enable cells to grow and interact within an environment that closely mimics the solid tumors' morphology and behavior [10]. Spheroids and organoids act as a bridge between monolayer cell cultures and *in vivo* models, offering a more accurate representation of the complex cellular interactions and gradients present in solid tumors [11]. Moreover, some tumor spheroids from primary cells have demonstrated the ability to produce a capsule-like endogenous ECM, which effectively replicates the solid tumor microenvironment [12]. Furthermore, as the diameter of the spheroid increases, the outer layers receive nutrients and oxygen, while the inner core suffers from hypoxia, modulating gene expression, such as the activation of HIFs [13]. Among the various types of spheroids, multicellular tumor spheroids (MCTS), composed of different cytotypes, most effectively mimic *in vivo* tumor gene expression, signaling, and cellular heterogeneity [14]. MCTSs have been developed using numerous tumor cells, including those from breast [11], lung [15], ovarian [16,17], liver [18], bladder [19], or prostate cancers [20]. To replicate the TME, and particularly the tumoral angiogenesis, Human Umbilical Vein Endothelial Cells (HUVECs) were

incorporated into MCTS, alongside various tumor cell lines, resulting in capillary-like structures [21–23].

While HUVECs form vessel-like structures that closely resemble the *in vivo* biological arrangement, it is challenging to fully replicate the entire microvascular network, which consists of capillaries, venules, arteries, and accessory cells. A promising solution to this limitation is the involvement of Microvascular Fragments (MVs), which comprise intact vessel fragments, including capillaries, arteries, and veins. They retain the essential endothelial framework and are associated with accessory cells, such as pericytes, mesenchymal stem cells, progenitor cells, and macrophages [24,25]. Microvascular fragments can be isolated from adipose tissue [26], a readily available and abundant source that allows for a straightforward isolation procedure. When cultured, MVs secrete growth factors like VEGF and FGF, promoting rapid microvessel growth and the formation of functional microvascular networks capable of connecting with host tissue upon implantation [25,27,28]. For the first time, Nalbach and colleagues created MVF-derived spheroids that demonstrated angiogenic activity and *in vivo* vascularization capacity, suggesting their potential as vascularization units for future tissue engineering applications [29]. Subsequently, MVs have been used to create adipose spheroids that demonstrated the ability to sprout and form a new vascular network [30], as well as to reconstruct subcutaneous adipose tissue when transplanted into *in vivo* localized scleroderma patients, where they fostered an anti-fibrotic and pro-adipogenic microenvironment that aided the regeneration of scleroderma lesions [31]. Moreover, MVs have been combined with osteoblasts to generate spheroids, which, in this context, exhibited sprouting and inosculation capabilities when implanted into an *in vivo* murine model [32].

In this study, a novel 3D spheroid model named "angiotumoroids" was generated, combining primary murine breast tumor cells with species-specific MVs extracted from adipose tissue. They exhibit endothelial integration, enhanced MMP9, vessel sprouting, and altered doxorubicin uptake with reduced cytotoxicity. These features make angiotumoroids a physiologically relevant "in vitro"

platform for studying tumor–vascular interactions, angiogenesis, drug response, and therapeutic resistance in cancer research.

Methods

Rat model

All animal experiments were approved by the University of Palermo. Authorization n° 523/2022-PR, issued according to art. 31 del D.lgs. 26/2014 Istituto Superiore di Sanità, Italy. Female Wistar rats were obtained from ENVIGO RMS SRL.

Microvascular Fragments (MVs) Isolation

MVs were isolated from female Wistar rat visceral adipose tissue [33]. The animal was sedated with 2% Isoflurane, sacrificed and the adipose tissue from abdominal region was explanted and put in Dulbecco's Modified Eagle's Medium high glucose (HG-DMEM, Sigma-Aldrich, Milano, Italy) added of penicillin 15.000 U/ml, streptomycin 300 µg/ml, and amphotericin B 0.75 µg/ml (Sigma-Aldrich, USA). The adipose tissue was washed 3 times in Phosphate Buffered Saline (PBS) w/o Ca²⁺ and Mg²⁺, then dissected into small parts with a scalpel. Furthermore, the tissue was incubated with the digestion buffer, containing ultrapure recombinant collagenases class II (Col H 300 U/gr) (Abiel srl) and Thermolysin (Promega) 10µg/ml. The digestion was performed at 30°C for 30 min under agitation. After 30 minutes, the tissue was mixed and digested for further 20 minutes at 30°C. The digestion was then stopped with HG-DMEM containing 10% (v/v) fetal bovine serum (FBS, Euroclone, Celbar, Pero (MI) Italy). The sample was washed three times with HG-DMEM and centrifuged at 700g for 10 minutes to isolate MVs from the adipose tissue. The MVs pellet was resuspended in HG-DMEM added of penicillin 15.000 U/ml, streptomycin 300 µg/ml, and amphotericin B 0.75 µg/ml, 2 mM L-Glutamine (Euroclone, Celbar, Pero (MI) Italy) and 10% (v/v) FBS, and filtered through a mesh (300 µm). The resulting MVs were counted in a Burker's chamber.

Primary Tumor Cells (PTCs) and MVFs 3D co-culture

PTCs isolated from a breast tumor mass [12] were cultured in HG-DMEM plus 1% penicillin/streptomycin, 1% L-Glutamine and 10% FBS (complete HG-DMEM). Cells were maintained at 37 °C in a humidified atmosphere with 5% CO₂. To form angiotumoroids, PTCs from passages 15 to 19 and isolated MVFs were co-cultured in a 96-well low attachment plate in complete HG-DMEM, at 37 °C and 5% CO₂, and were allowed to grow for 5 days. Three co-culture formulations were obtained using the same PTCs density (3×10^3 cells) co-cultured with 60, 125, or 250 MVFs. Moreover, spheroids constituted only of MVFs (500 MVFs per spheroid) or only of PTCs (3×10^3 PTCs per spheroid) were formed and used as controls. The size and shape of angiotumoroids were investigated by optical microscopy and analyzed through ImageJ software.

Spheroids fixation and preparation for Scanning Electron Microscopy (SEM) imaging

Spheroids were washed with complete PBS (3 times for 3 minutes) and fixed with 4% Glutheraldehyde in PBS for one hour at 4°C. Samples were then washed in complete PBS (2 times for 3 minutes) and dehydrated with an increasing ethanol solution at room temperature (30%, 70%, 90%, and 100% in PBS, each wash for 5 minutes). After dehydration, 3D cultures were resuspended in hexamethyldisilazane (HMDS, Sigma-Aldrich, 379212) for 10 min for critical point drying. The stubs were covered with carbon tape onto which the samples were dried at room temperature. Then, the stubs were put into the sputter coater device (Quorum SC7620) to coat the samples with platinum for 15 seconds. The images were acquired in a high vacuum in Secondary Emission (SE) mode using SEM EVO 10 and analyzed using SmartSEM Touch software.

Immunofluorescence staining and imaging of spheroids and spheroids in collagen gels

Spheroids were fixed in 3,7% formaldehyde for one hour at room temperature before permeabilization in PBS supplemented with 0.1% triton X-100 (ON at 4°C). They were then

blocked for one hour at room temperature using PBS with 1% BSA (Sigma-Aldrich, A7906). The primary antibody used were Rabbit anti-CD31 (1:50, ab222783, Abcam), Rabbit anti-Collagen Type I (1:20, 234167, Millipore), Rabbit anti-Collagen Type IV (1:100, ab6586, abcam) and Mouse anti-ABCB1 (1:100, MA5-13854, Invitrogen), which were incubated overnight at 4°C in a blocking buffer. Spheroids were stained with the species-specific fluorophore-conjugated secondary antibody (Invitrogen) for four hours at room temperature. The Actin cytoskeleton was labeled with phalloidin-FITC (1:500 in PBS, Sigma-Aldrich, P5282) for 30 min at room temperature, while nuclei were labeled with DAPI (1:20.000 in PBS, Sigma-Aldrich, D9542). Coverslips were mounted in a mounting medium, and 3D cultures were analyzed by confocal microscope (Olympus FV10i). Z-stack imaging was carried out using a Fluoview FV10i confocal laser scanning microscope system (Olympus) at a magnification of 20x with a step size of 10µm. All stacks were obtained at the same intensity setting between groups. ImageJ software was used to analyze stacks of images.

Western Blot analysis

Cells from 3D cultures were lysed in RIPA buffer (20 mM Tris, 150 mM NaCl, 0.1% Triton X-100, 1 mM EDTA, pH 7.2) with a protease inhibitor cocktail. Lysates were incubated in a sample buffer under reducing conditions and fractionated with Sodium dodecyl sulphate–polyacrylamide gel electrophoresis (SDS–PAGE) 10% and transferred to nitrocellulose membranes (Amersham). The membranes were blocked in PBS/Tween 0.1% (PBS/T) with 5% non-fat dried milk, incubated with the primary antibody Rabbit anti-CD31 (1:1000, ab222783, abcam) or Rabbit anti-ABCB1(1:500, A808889, antibodies) diluted in PBS/T, washed four times in blocking solution and incubated with HRP-conjugated secondary antibodies (Sigma) followed by washing in PBS/T. The membrane was exposed to Super Signal West Femto Maximum Sensitivity substrate (Thermo Scientific), and protein expression was detected by ChemiDoc XRS (Biorad, Hercules, CA, USA).

Gelatin Zymography assay

15 µg of total proteins from 3D Cell lysates (as previously described) were analyzed by gelatin zymography in 10% acrylamide gels, containing 0.09% gelatin (SIGMA Aldrich, USA). Gel was washed for 10 minutes in 2.5% Triton X-100 at room temperature and incubated overnight at 37°C in activation buffer (50 mM Tris-HCl, 2 mM CaCl₂, NaN₃ 0.02%, Triton X100 1,5%). Gel was stained for 1 hour with Coomassie Brilliant Blue R-250 (0.2% Coomassie Brilliant Blue R-250, 40% methanol, 10% acetic acid in H₂O) and destained in H₂O. White bands were quantified using ImageJ software.

Collagen gel for embedding of MVFs and angiotumoroids and sprouting analysis

The isolated MVFs, angiotumoroids and control spheroids were embedded in a collagen gel composed of 35,3% Buffer solution (PBS 2X, 100 mM HEPES, pH 7.4), 35,3% type I collagen from rat tail (3 mg/ml), and 29,4% of complete HG-DMEM [34]. The isolated MVFs (iMVFs) were grown in collagen gel for 1 week, while angiotumoroids and control spheroids (MVF and PCT) were embedded for 2 days. The number of sprouts was quantified by analyzing optical microscopy images with ImageJ software.

Treatments with conditioned media from PTCs and sprouting analysis after treatment

The MVF spheroids were embedded in collagen gel and treated with a PTC-conditioned medium recovered from 30.000 PTC cells grown in 2D monolayer condition. As a control, MVF spheroids were embedded in collagen gel and grown in complete HG-DMEM. On day 1 and day 2, the number of sprouts was quantified by analyzing optical microscopy images with ImageJ software.

Proteomic-based characterization: protein extraction and sample preparation

Angiotumoroids, PTC and MVFs spheroids were lysed in STET (10 mM Tris-HCl, 1 mM EDTA, 100 mM NaCl, and 5% Triton X-100 (v/v)) with protease inhibitor cocktail (Roche) and centrifuged

(14,000 rpm, 5 min) to eliminate cells membranes. Proteins extracted were quantified with colorimetric 660 nm microBCA assay. A protein amount of 30 μg per sample was subjected to filter-aided sample preparation (FASP - with 10 kDa Vivacon 500 spin filter columns from Sartorius), as previously described [35]. Samples were then reduced and denatured with dithiothreitol (DTT) (Sigma-Aldrich) in 200 μl of UA buffer (8M Urea in 0.1 M Tris/HCl, pH 8.5) and alkylated with 50 mM iodoacetamide (IAA) (Sigma-Aldrich). After reduction and alkylation, samples were washed three times with UB buffer (8M Urea in 0.1 Tris/HCl, pH 8.0) and sequentially digested with LysC (1:50 enzyme to protein ratio from Promega) and trypsin (1:100 enzyme to protein ratio, Promega). Then, peptides were eluted from filter columns by centrifugation (14,000 \times g; 60 min) and acidified with 20 μl of 8% formic acid (FA). Generated peptides were desalted by stop-and-go extraction (STAGE) on reverse phase C18 and eluted in 40 μl of 60% acetonitrile in 0.1% formic acid [36]. The volume was reduced in a SpeedVac (Thermo Fisher Scientific) and the peptides were resuspended in 20 μl of 0.1% formic acid. The peptide concentration was measured with Nanodrop 2000 (Thermo Scientific)

uHPLC-MS/MS and data analysis

As previously described [37] for each sample 1 μg peptides were separated through a nanoLC system (Vanquish Neo UHPLC, Thermo Scientific) equipped with an Acclaim PEPMap C18 column (25 cm \times 75 μm ID, Thermo Scientific) in a 110 min binary gradient of water and acetonitrile containing 0.1% FA. Separated peptides were injected into an Exploris 480 mass spectrometer (Thermo Fischer Scientific) for tandem mass spectrometry analysis. Proteins were identified and quantified with label-free quantification (LFQ), by using data-independent acquisition (DIA). DIA was performed using an MS1 full scan (380 m/z to 980 m/z) followed by 49 sequential DIA windows with an overlap of 1 m/z and window placement optimization option enabled. Full scans were acquired with 120,000 resolution, AGC of 3×10^6 , and a maximum injection time of 50 ms. Afterward, 49 isolation windows were scanned with a resolution of 30,000,

an AGC of 8×10^5 and maximum injection time was set as auto to achieve the optimal cycle time. Collision-induced dissociation fragmentation was induced with 28% of the normalized HCD. The data were analyzed by the software DIA-NN (version 2.0.2) by using a predicted library generated from *in silico* digested *Rattus norvegicus* (rat) Uniprot reference database (proteome ID UP000002494) involving cuts at K* and R*, two missed cleavage allowed, minimal peptide length set a 6. The false discovery rate for peptide and protein identification was set at 0.01%. Label-free quantification (LFQ) was used for protein quantification. The LFQ values were log₂ transformed and a two-sided Student's t-test was used to evaluate proteins statistically significantly regulated between two-dimensional and three-dimensional culture (n=4). The mass spectrometry proteomics data have been deposited to the ProteomeXchange Consortium via the PRIDE partner repository with the dataset identifier PXD067876.

Doxorubicin uptake study by confocal microscopy

To assess the uptake of Doxorubicin, angiotumoroids with 125 MVFs and PTC spheroids were incubated with 10 μ M Doxorubicin for 30 minutes, 1h, 2h, or 4h. Spheroids were then processed for immunocytochemistry, as previously described, and analyzed with Fluoview FV10i confocal laser scanning microscope system (Olympus). ImageJ software was used to analyze stacks of images.

Cell Viability Assay

Angiotumoroids with 125 MVFs and PTC spheroids were incubated with 10 μ M Doxorubicin for 24h at 37°C in a humidified atmosphere with 5% CO₂. After treatment, spheroids were washed three times with PBS, resuspended in 100 μ l of DMEM and an equal volume of CellTiter-Glo® 3D Reagent (Promega) following the Manufacturer's protocol. Briefly, 100 μ L medium was replaced with 100 μ L CellTiter-Glo 3D reagent on the indicated day after growth/treatment. The plates were shaken for 5 min at 240 rpm, and incubated for 25 min at room temperature, and the luminescent signal was recorded using a luminometer (SinergyHT, BioTek, Winooski, VT, USA).

Statistical analysis

The results are presented as the mean \pm standard deviation (SD). Statistical comparisons were made using one-way ANOVA and 2-way ANOVA. Statistical tests were performed with GraphPad Prism. A p-value <0.05 was considered statistically significant.

Results

Adipose-derived microvascular fragment isolation and 3D co-culture with primary tumor cells

Microvascular Fragments (MVs) were isolated from visceral adipose tissue of female Wistar rats (Figure 1A). The tissue was digested using a blend of ultrapure recombinant collagenase (COLH - Class II) and thermolysin as reported in the materials and methods section, yielding approximately 20,000 MVs per gram of adipose tissue. MVs ranged in length from 50 μm to 300 μm , with an average lumen diameter of 18 μm . They displayed small lateral branches and retained traces of blood within their lumen (Figure 1B). Scanning Electron Microscopy (SEM) analysis (Figure 1C) revealed the tubular structure of isolated MVs and the presence of erythrocytes in vessels, while adipocytes were absent, indicating the efficiency of the isolation protocol in removing adipose tissue. Isolated MVs were embedded in a type I collagen gel and maintained for seven days to assess their viability. After 3 days, isolated MVs showed vessel sprouting and branching, which progressively increased in number and network complexity over time (Figure 1D). Furthermore, after seven days, some lateral branches derived from different fragments were fused, mimicking *in vitro* the angiogenic process that typically occurs *in vivo*.

To develop a reliable and reproducible *in vitro* tumor model with a well-organized and natural TME, primary tumor cells (PTC) from a rat breast tumor mass were combined with MVs. The PTCs and the MVs were seeded in low-attachment conditions to develop three-dimensional (3D)

in vitro structures named “angiotumoroids”. Angiotumoroids were generated by varying the number of MVFs in culture (60, 125, or 250 MVFs), while maintaining the number of PTC constant (3×10^3 cells/well) per condition. Additionally, spheroids consisting of only MVFs, or PTCs were formed as controls.

Optical microscopy analyses were performed to investigate spheroid structure and size evolution from 0 to 5 days post-seeding (Figure 1E). PTC spheroids were formed one day after seeding, exhibiting a compact and well-defined structure that was maintained over time. All angiotumoroid formulations (+60, +125, and +250 MVFs) were also formed by day 1 and showed increased compaction in a time-dependent manner, while MVF spheroids spent five days organizing themselves, suggesting a significant role for PTCs in driving the process of formation of spheroidal structures.

As expected, angiotumoroids presented a larger diameter compared to the controls. However, at 5 days post-seeding, those with 250 MVFs were less homogeneous in size compared to the other conditions, with diameters ranging from 200 μm to 445 μm (Figure 1F). This variability is probably due to an excess of MVFs compared to PTCs, leading to the formation of "satellite" structures that partially sequester the PTCs. Therefore, to better investigate component integration and morphology, both angiotumoroids and controls were analyzed by SEM at day 5 (Figure 1G). PTC spheroids, along with those containing 60 and 125 MVFs, and with MVF-only spheroids, exhibited a similar morphology, with a compact ovoid structure and rounded cells on the surface. In contrast, spheroids with 250 MVFs had a distinct morphology, characterized by cells on the surface not perfectly integrated, suggesting a lack of structural compactness.

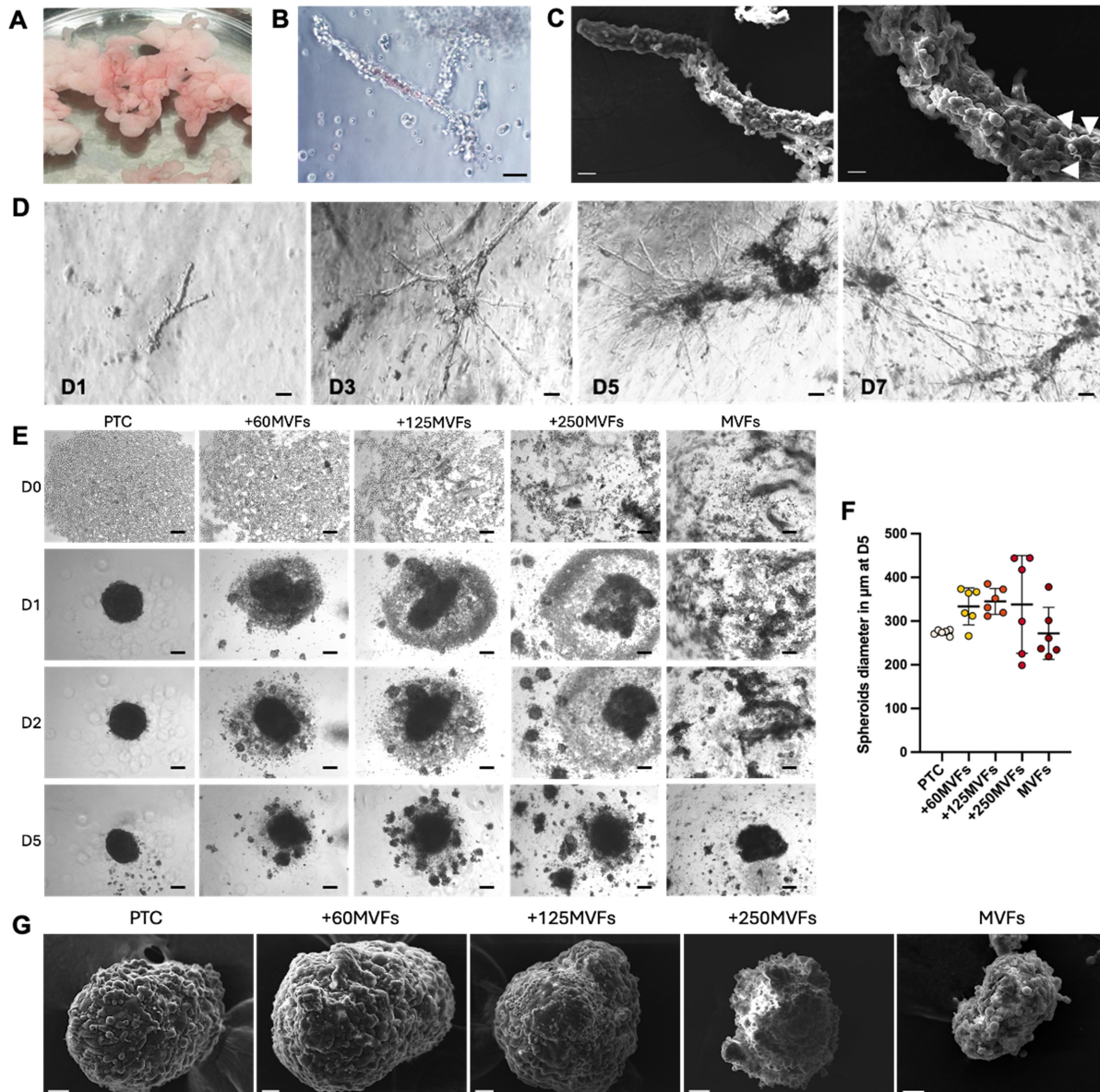


Figure 1. Adipose-derived microvascular fragment isolation and 3D co-culture with primary tumor cells. (A) Rat visceral adipose tissue. (B) MVFs analysis through optical microscopy and (C) Scanning Electron microscopy (SEM), Scale bar: 20 μm and 10 μm , respectively. White arrows indicate the erythrocytes. (D) Isolated MVFs included in type I collagen gel at days 1 (D1), 3 (D3), 5 (D5), and 7 (D7). Scale bar: 10 μm . (E) Optical microscope analysis of primary tumor cell spheroids (PTC), angiotumoroids with 60 (+60MVFs), 125 (+125MVFs), or (+250MVFs) 250 MVFs and MVF spheroids at days 0 (D0), 1 (D1), 2 (D2), and 5 (D5). Scale bar: 100 μm . (F)

Spheroid diameter analysis on day 5. Six spheroids were analyzed for each condition. Data are mean \pm SD. (G) SEM analysis of spheroid on day 5. Scale bar: 30 μ m.

Integration of microvascular fragments into angiotumoroids correlates with increased MMP9 expression

To evaluate the presence and distribution of MVFs within the 3D structures, both angiotumoroids and controls were analyzed for the expression of the endothelial vascular marker CD31 (Figure 2A). At day 5, CD31 was uniformly distributed in both MVF and angiotumoroid spheroids, while no signal in the PTC spheroids was detected. Notably, angiotumoroids exhibited a gradual increase in CD31 expression throughout the structure, directly correlated to the number of MVFs seeded per spheroid.

Furthermore, MVFs successfully integrated into the angiotumoroids, forming vasculature-like structures (Figure 2B). These data were also confirmed by western blot assay, in which it is evident that the CD31 signal increased in a MVF density-dependent manner (Figure 3C).

Since matrix metalloproteinases (MMPs), particularly MMP9, are directly involved in tumor angiogenesis, zymography assays were carried out on the total proteins isolated from angiotumoroids and control spheroids (Figure 2D). MMP expression patterns were compared to those of PTC spheroids (Figure 2D). The MMP complex activity was proportionally augmented in angiotumoroids as the number of MVFs increased, while it was significantly less in PTC spheroids (Figure 2E). The catalytic activity, induced by the zymography process, of pro-MMP9 was significantly enhanced in angiotumoroids with 125 and 250 MVFs and MVF spheroids compared to the PTC spheroids, which exhibited three times lower activity (Figure 2F). Interestingly, the enzymatic activity of active-MMP9 was notably higher in angiotumoroids with 125 and 250 MVFs compared to PTC spheroids, an increase not observed in the MVFs spheroids (Figure 2G), suggesting a potential effect due to a crosstalk between PTC/MVFs co-culture. Additionally, MMP2 activity analysis revealed no significant differences in the pro- and active forms between

angiotumoroids and MVFs or PTC spheroids (Figure 2H-I). Taken together, these data suggest that different amounts of MVFs combined with primary tumor cells may modulate the MMPs' activity differently, especially MMP9.

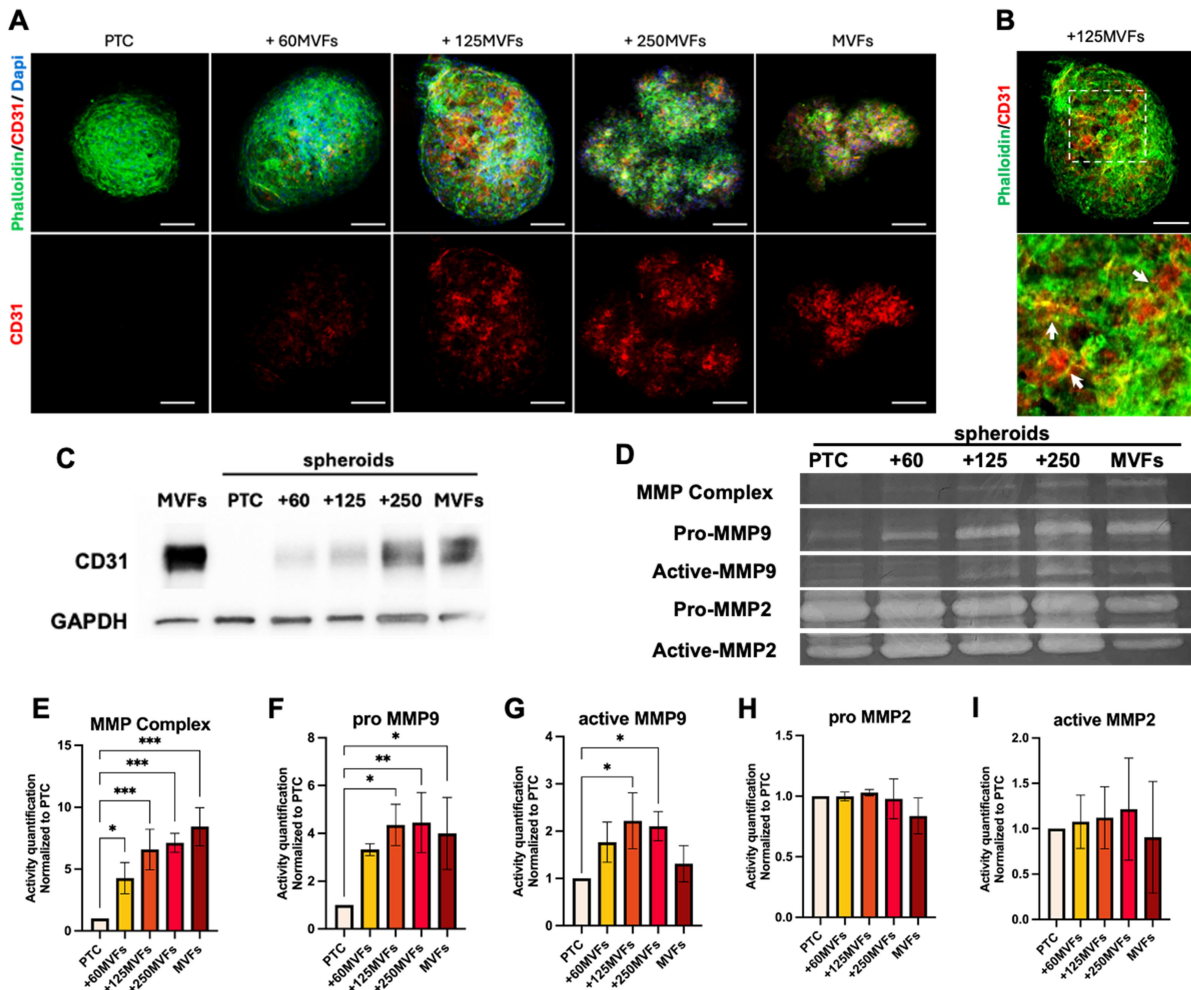


Figure 2. Integration of microvascular fragments into angiotumoroids correlates with increased MMP9 expression. (A) Confocal microscope of primary tumor cell spheroids (PTC), angiotumoroids with 60 (+60MVFs), 125 (+125MVFs), or 250 (+250MVFs) MVFs, and spheroids of MVFs, stained with phalloidin-FITC (green), anti-CD31 antibody (red), and DAPI (blue) at day 5. Scale bar: 100 μ m. (B) Central section at the confocal microscope of angiotumoroids with 125 MVFs, stained with phalloidin-FITC (green), and anti-CD31 antibody (red). Arrows point to

vasculature, CD31 positive. (C) Western blot analysis for CD31 and (D) Zymography assay of protein extract from PTC spheroids, angiotumoroids with 60 (+60MVs), 125 (+125MVs), or 250 (+250MVs) MVs, and MVs spheroids. (E-I) Quantification of the gelatinolytic activity of the samples. The matrix metalloproteases (MMPs) analyzed were: MMP complex (E); pro-MMP9 (F); active MMP9 (G); pro-MMP2 (H); active MMP2 (I). Data are mean \pm SD. Statistical analysis (one-way ANOVA) was performed (n=3) (*p < 0.05; **p < 0.01).

Angiotumoroids sprouting in collagen gel and the influence of PTCs in neoangiogenesis.

To investigate the neo-angiogenic process in angiotumoroids, they were embedded in 3D collagen gel. Vessel sprouting was evaluated through optical microscopy up to 2 days post-embedding (Figure 3A). As expected, the PTC spheroids exhibited a loss of compactness and integrity over time, given by cell migration into the gel, with no vessel formation observed. Angiotumoroids with 60 and 125 MVs and MVs spheroids showed visible sproutings on the first day after embedding, which increased the following day (day 2). Interestingly, angiotumoroids with 60 and 125 MVs presented a higher number of newly formed vessels and branching than MVs spheroids (Figure 3B), suggesting an effect on the crosstalk between tumor cells and MVs. Moreover, angiotumoroids with 125 MVs generated longer sprouts than those with 60 MVs, reaching lengths at day 2 comparable to those observed in MVs spheroids (Figure 3C). In contrast, angiotumoroids with 250 MVs exhibited rounded cells surrounding the spheroids on the same embedding day, suggesting reduced compactness relative to other conditions. Therefore, by the first day, only a few new vessels had sprouted, with single cells migrating outward, and no increase in sprout number was observed on day two compared to day one.

Although both 125 MVs and 250 MVs presented high active MMP9 levels, these data showed that only 125 MVs can sprout and branch after embedding in collagen gel. By contrast, 60 MVs spread in a 3D gel despite showing a slightly lower expression of active MMP-9. Furthermore, when two 125 MVs angiotumoroids were cultured within the same collagen gel, interconnection

between them was observed after 2 days, with new vessel formation extending to connect with sprouts from neighboring spheroids (Figure 3D).

To determine whether the pro-angiogenic effects of PTCs on vessel sprouting were due to direct contact interactions or the release of soluble factors, MVF spheroids were embedded in collagen gels and treated with a PTC-conditioned medium (Figure 3E). Optical microscopy images were acquired up to two days post-treatment. After 24 hours, sprouts in spheroids treated with the conditioned medium increased by 2.2-fold compared to MVF control spheroids. Notably, after 48 hours, this difference became statistically significant (Figure 3F). Additionally, the analysis of vessel branching revealed increased ramification of the sprouts in MVF spheroids treated with conditioned media (Figure 3G). These data confirm the direct involvement of PTCs in modulating the angiogenic process in angiotumoroids, highlighting the role of soluble factors released by PTCs in promoting neoangiogenesis.

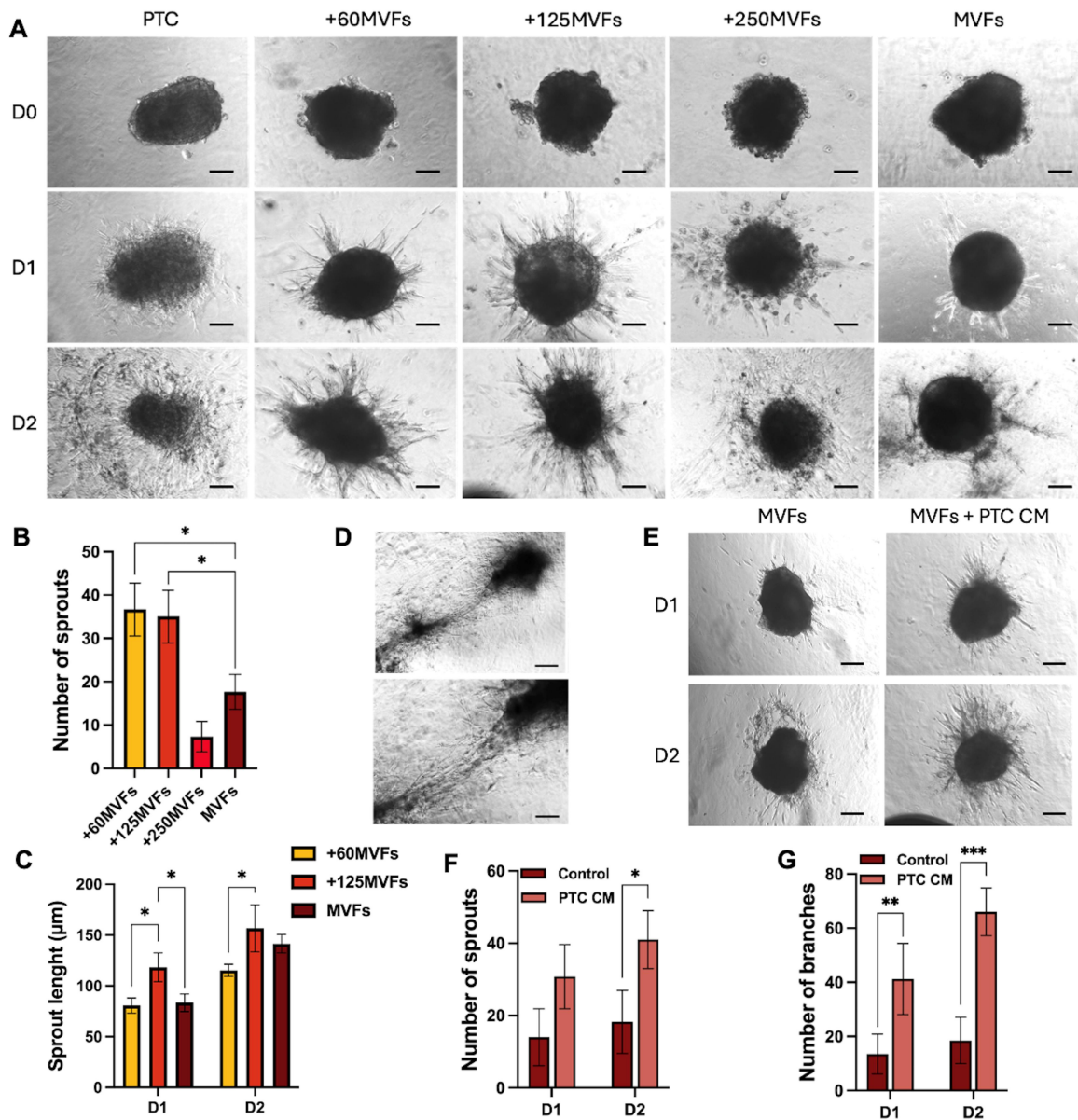


Figure 3. Angiotumoroids sprouting in collagen gel and the influence of PTCs in neoangiogenesis. (A) Primary tumor cell spheroids (PTC), angiotumoroids with 60 (+60MVFs), 125 (+125MVFs) or 250 (+250MVFs) MVFs and spheroids of MVFs in collagen gel at day 0 (D0), day 1(D1) and day 2 (D2). Scale bar: 100 μm (B) Quantification of the number of sprouts at D2 and (C) length of sprouts at D1 and D2. Data are mean \pm SD. Statistical analysis (2-way ANOVA) was performed ($n=3$) (* $p < 0.05$). (D) Angiotumoroids with 125 MVFs (+125 MVFs) interconnected in collagen gel. Scale bar: 50 μm and 25 μm for the magnification, respectively. (E) MVF spheroids

incubated in collagen gel with control DMEM (MVs) or with primary tumor cell conditioned medium (MVs +PTC CM) at day 1 (D1) and day 2 (D2). Scale bar: 100 μ m. (F) Quantification of the number of sprouts (G) and branches at D1 and D2 in MVs spheroids incubated in collagen gel with control DMEM (Control) or with primary tumor cells conditioned medium (PTC CM). Data are mean \pm SD. Statistical analysis (2-way ANOVA) was performed (n=3) (*p < 0.05; **p < 0.01; ***p < 0.001).

Proteomic profiling reveals vascular-specific tumor microenvironment remodeling and ABCB1 upregulation in angiotumoroids

Angiotumoroids with 125 MVs emerged as the most robust and reliable vascularized tumor models, based on their structural integrity, capacity to modulate MMP9 activity, and ability to promote new vessel sprouting and branching. To further characterize these models, high-resolution proteomic analysis was performed on angiotumoroids, PTC spheroids, and MVF spheroids, with a particular focus on proteins involved in angiogenesis, ECM composition, and remodeling. The analysis identified 5629 total proteins (of which 27 proteins are involved in angiogenesis, 60 in ECM composition and remodeling – according to Perseus software). (Supplementary Table 1). Principal Component analysis (PCA) demonstrated that the proteomic profiling of angiotumoroids was clearly separated from that of MVF spheroids and of PTC spheroids (Figure 4A). We used label-free quantification to evaluate the relative abundance of proteins in angiotumoroids compared to PTC and MVF spheroids. Label-free quantification was used to evaluate the relative abundance of proteins in angiotumoroids compared to PTC and MVF spheroids. 5093 proteins were found in angiotumoroids and PTC spheroids, of which 1587 significantly altered between the two samples (Figure 4B). 773 proteins were significantly more abundant in angiotumoroids than in PTC spheroids, including MMP9, in line with previous results, and other proteases involved in ECM turnover, such as MMP13, MMP10, and A disintegrin and metalloproteinase with thrombospondin motifs 1 (ADAMTS1). Furthermore, among increased proteins, there were proteins involved in

metabolic processes such as the platelet glycoprotein 4 (CD36), Adiponectin d (Adipoq) and the vascular endothelial growth factors A (VegfA). 814 proteins were less abundant in the angiotumoroids compared to the PTC spheroids. Among these, a group of proteins located in the inner membrane of the mitochondrion and involved in cellular respiration were the most altered (including NDUFS1, NDUFV1, NDUFV2, NDUFB7, FOXRED1, etc), as also proteins of the ECM such as Chondroitin Sulfate Proteoglycan 4 (CSPG4) and Collagen type I (Col1a1).

When angiotumoroids were compared with MVF spheroids, the relative abundance of 2342 proteins was significantly altered (Figure 4C). 1070 proteins increased in angiotumoroids, including stefin A2-like 1 (Stfa211), Protein S100-G (S100g) and some protein transporters, including the phospholipid-transporting ATPase (Atp8a1), sodium- and chloride-dependent taurine transporter (Slc6a6), and two subunits of the Sodium: Potassium-Exchanging ATPase Complex (Fxyd2 and Atp1b1). Notably, several ECM remodeling proteins were more abundant, such as MMP3, MMP10. In contrast, 1272 proteins were decreased in angiotumoroids compared to MVFs spheroids, including several ECM-related proteins such as the extracellular superoxide dismutase [Cu-Zn] (SOD3), collectin-12 (COLEC12), tenascin-C (Tnc), and fibrillin-1 (Fbn1).

Relative quantification of angiogenesis-related proteins, based on UniProt Gene Ontology annotations, revealed marked differences among the models. Specifically, six angiogenic proteins, including neuropilin-1 (NRP1) and MMP2, were significantly decreased in angiotumoroids. In contrast, five proteins were significantly upregulated compared to PTC spheroids, such as VEGFA and Epiregulin (EREG), highlighting a tumor cell-mediated pro-angiogenic profile. When compared to MVF spheroids, only two proteins, protein kinase C alpha (referred to as PRKCA by gene name) and Protein Tyrosine Kinase 2 Beta (PTK2B), were significantly augmented (Figure 4D). These proteomic differences suggest that angiotumoroids represent a distinct biological model with features that diverge from both PTC and MVF controls. Notably, angiotumoroids not only contain MVFs with angiogenic sprouting potential but also exhibit enhanced ECM composition and remodeling, as revealed by proteomics analysis (Figure 4E). Remarkably, ECM components such as

Collagen Type I and Collagen Type IV remained abundant in the vascularized tumor model (Figure 4F), supporting the presence of a structurally rich ECM. In parallel, a more complex ECM remodeling scenario was indicated by increased levels of several MMPs, including MMP3, MMP9, MMP10, MMP11, and MMP13 (Figure G), underscoring the critical roles these enzymes play in promoting tumor angiogenesis and matrix degradation.

Furthermore, proteomic analysis identified altered expression of several ATP-binding cassette (ABC) transporters, with ABCB1 (P-glycoprotein) being significantly more abundant in angiotumoroids compared to both PTC and MVF controls (Figure H). Given ABCB1's well-established role in drug efflux and chemoresistance [38], its elevated expression suggests that angiotumoroids may also serve as a relevant platform for studying drug distribution and resistance mechanisms within a vascularized TME.

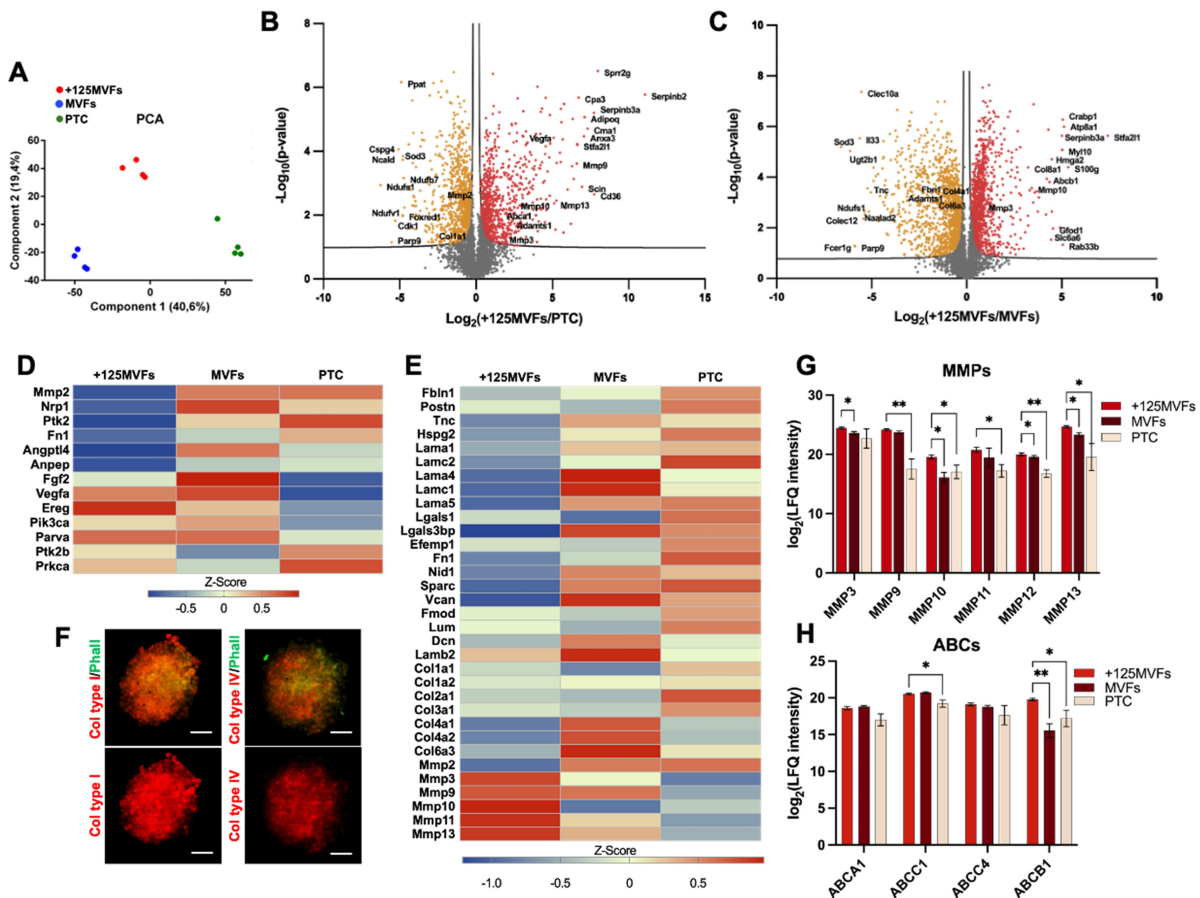


Figure 4. (A) Principal Component analysis (PCA) of 125 MVFs (+125MVFs), spheroids of MVFs, and primary tumor cell spheroids (PTC). (B) Volcano plot for the proteins identified in four biological samples of +125MVFs and MVFs. (C) Volcano plot for the proteins identified in four biological samples of +125MVFs and PTC. (D) Heatmap generated based on protein z-scores in angiotumoroids with 125 MVFs (+125MVFs), spheroids of MVFs and primary tumor cell spheroids (PTC) involved in angiogenesis (E) and ECM composition and remodelling. (F) Confocal microscope of primary tumor cell spheroids (PTC), and angiotumoroids with 125 (+125MVFs) stained with phalloidin-FITC (green), antibody anti-Collagen Type I or Collagen Type IV (red) at day 5. Scale bar: 100 μ m. (G) LFQ (label-free quantification) intensity of the most significant MMPs (Matrix Metalloproteinases) (H) and ABC transporters differentially expressed in angiotumoroids with 125 MVFs (+125MVFs), spheroids of MVFs and primary tumor cell spheroids (PTC) (n=4).

ABCB1 expression and drug sequestration in angiotumoroids

To investigate the expression and distribution of ABCB1 in angiotumoroids containing 125MVFs, western blot analysis was performed, confirming a significant upregulation of ABCB1 protein compared to PTC spheroids (Figure 5A). Consistently, immunofluorescence staining revealed minimal ABCB1 expression in PTC spheroids, whereas in angiotumoroids, ABCB1 was clearly localized to both endothelial and tumor cell compartments, indicating a broader functional role within the vascularized tumor microenvironment (Figure 5B).

To assess drug accessibility and cytotoxic response in this model, angiotumoroids were treated with doxorubicin five days post-formation, and viability was assessed 24 hours after drug exposure. Compared to PTC spheroids, which exhibited widespread cell death, angiotumoroids maintained a more compact structure (Figure 5C). Quantitative analysis revealed a significantly higher survival

rate in angiotumoroids (60%) compared to PTC spheroids (23%) (Figure 5D), indicating that doxorubicin may be partially retained or sequestered within the angiotumoroid structure, potentially limiting its cytotoxic penetration and efficacy.

To further explore the role of MVFs on drug distribution, doxorubicin uptake was monitored over time (30 min, 1 h, 2 h, and 4 h) by measuring doxorubicin autofluorescence in angiotumoroids and PTC spheroids (used as controls; Figure 5E). Both models exhibited a time-dependent increase in fluorescence intensity, indicating progressive intracellular drug accumulation. However, angiotumoroids displayed a markedly stronger fluorescent signal already after 30 minutes of incubation (Figure 5F), suggesting facilitated drug uptake or compartmentalization in specific regions. Importantly, fluorescence in angiotumoroids was predominantly localized to MVF-rich regions, as confirmed by colocalization with the endothelial marker CD31 (Figure 5G). This spatial distribution suggests that the vascular components within the angiotumoroids may play an active role in modulating drug distribution and local transport dynamics, contributing to a more physiologically relevant tumor microenvironment.

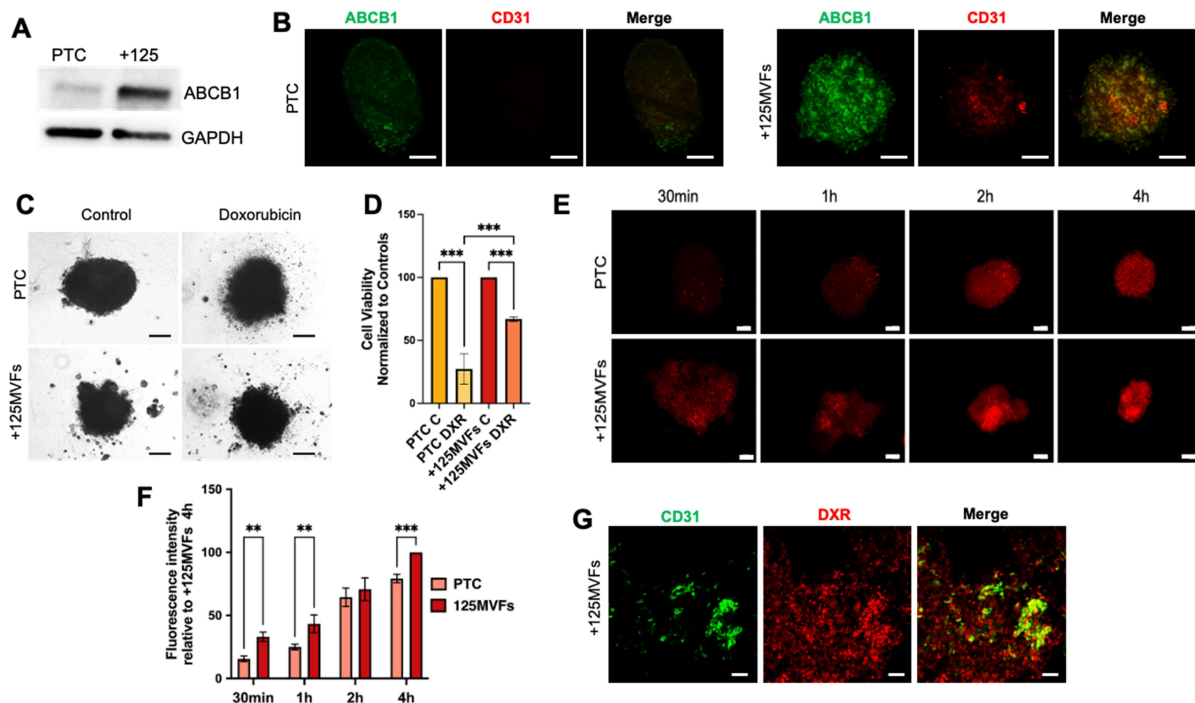


Figure 5. ABCB1 expression and drug sequestration in angiotumoroids. (A) Western blot analysis for ABCB1 in Primary tumor cell spheroids (PTC) and angiotumoroids with 125 MVFs (+125MVFs). (B) Confocal microscope of primary tumor cell spheroids (PTC), angiotumoroids with 125 (+125MVFs) MVFs stained with anti-ABCB1 antibody (green) and anti-CD31 antibody (red) at day 5. Scale bar: 100 μm . (C) Primary tumor cell spheroids (PTC) and angiotumoroids with 125 MVFs (+125MVFs) after 24h of treatment with 10 μM doxorubicin. Scale bar 100 μm . (D) Cell viability assay of primary tumor cell spheroids (PTC) and angiotumoroids with 125 MVFs (+125MVFs) after 24h of treatment with 10 μM doxorubicin (DXR). PTC C and +125MVFs C are the controls (not treated spheroids). Data are mean \pm SD. Statistical analysis (2-way ANOVA) was performed (n=3) (**p < 0.01). (E) Fluorescence analysis of 10 μM doxorubicin uptake in primary tumor cell spheroids (PTC) and angiotumoroids with 125 MVFs (+125MVFs) at different time points (30 min, 1h, 2h, 4h). Scale bar: 30 μm . Red: doxorubicin autofluorescence. (F) Quantification of the fluorescence intensities was analyzed and normalized to +125MVFs at 4h. Data are mean \pm SD. Statistical analysis (2-way ANOVA) was performed (n=3) (**p < 0.01). (G) Angiotumoroids with 125 MVFs stained with anti-CD31 antibody (green) and doxorubicin (red). Scale bar: 200 μm .

Discussion

Solid tumors are characterized by a highly complex microenvironment composed of tumor vasculature, connective tissue, infiltrating immune cells, and the tumor extracellular matrix (TEM) [39]. Given the intricate nature of tumor biology and the limitations of traditional two-dimensional culture models, three-dimensional (3D) tumor spheroids have emerged as a more relevant model for cancer research *in vitro*, making them invaluable for investigating cancer characteristics, progression, drug responses, and therapeutic resistance. 3D models can mimic solid tumor structures, developing features like a hypoxic core [13] and an ECM [12] that partially recreates the

tumor microenvironment (TME). However, the TME extends beyond the extracellular matrix, encompassing various associated cells, including cancer-associated fibroblasts and tumor-associated macrophages, as well as a functional vascular network. Angiogenesis is essential for tumor growth and metastasis, making its accurate replication in 3D models a key step toward achieving *in vivo* conditions. While many studies have incorporated endothelial cells (e.g., HUVECs) into tumor spheroids [23,40], the resulting vascular networks often remain underdeveloped. To address these limitations, this study aimed to develop a novel model incorporating murine adipose-derived microvascular fragments (MVs) alongside primary murine breast cancer cells (PTCs). MVs are intact fragments of blood vessels comprising a mixture of capillaries, veins, and arteries. They retain all the defining features of fully formed blood vessels, including accessory cells, such as pericytes [26]. In research, MVs have been widely used to establish functional vascular networks within collagen matrices. They have demonstrated the ability to integrate with the host's circulatory system following transplantation, ensuring graft survival by facilitating the delivery of oxygen and nutrients, and removing metabolic toxic products [27]. Isolated MVs have been employed to generate 3D spheroids, either alone or in combination with other cell types such as adipocytes or osteoblasts [32]. Furthermore, human MVs have been used to model tumor angiogenesis by placing them adjacent to colorectal cancer spheroids [41]. Based on the unique capabilities of MVs, this study explores their use as a tool to more accurately mimic the TME. To achieve this goal, an essential initial step was the development of a well-defined and reproducible protocol for isolating MVs from the visceral adipose tissue of Wistar rats. Structural analysis by scanning electron microscopy (SEM) confirmed the complete removal of surrounding adipose tissue and revealed a clean vascular morphology. The MVs not only preserved their structural integrity but also exhibited sprouting and branching activity.

To develop a more physiologically relevant *in vitro* tumor model, PTCs isolated from rat mammary tumors were combined with MVs to form 3D models referred to as "angiotumoroids". By varying the number of MVs included in the model (60, 125, or 250) while maintaining a constant number

of PTCs, we aimed to explore the impact of the vascular system on the structural organization and potential functionality of these models. The addition of MVFs significantly affected the angiotumoroids' structural development over time. Constructs with the highest MVF number (250) exhibited increased size variability and a less compact morphology, indicating that an excessive vascular load might hinder the self-organizing ability of tumor cells. SEM analyses revealed notable differences in structural integrity. Angiotumoroids with intermediate MVF content showed a cohesive and well-organized architecture, characterized by closely packed cell populations and integrated microvascular elements. Conversely, angiotumoroids with 250 MVFs revealed surface cells that were not fully incorporated into the structure; probably, due to the excess of satellite microvessels that sequester part of the PTCs, preventing the formation of angiotumoroids with a compact structure. Interestingly, angiotumoroids required approximately five days to compact, and this temporal delay is in contrast with PTC spheroids, which became compact earlier and displayed a more uniform structure from the initial stages. This suggests that while MVFs enrich the biological relevance of the model, their inclusion also adds complexity, impacting the kinetics of tissue-like organization. Overall, these findings indicate a need to balance the use of vascular components to improve the physiological relevance while preserving the structural integrity essential for reliable analysis. The angiotumoroids, particularly those composed of an intermediate MVF density, provide a valuable tool for exploring tumor–vasculature interactions and developing more predictive systems in therapeutic approaches.

The integration of the MVFs into 3D angiotumoroid models leads to a progressive formation of vascular-like structures, indicated by CD31 positivity [42]. The increase in CD31 expression with a higher number of MVF, evidenced through both immunofluorescence and western blot analyses, confirms successful integration of endothelial structures and the potential formation of a vascular-like network within the angiotumoroids. In these models, MVFs and tumor cells crosstalk modulate proteolytic activities, especially those involved in angiogenesis. MMPs, particularly MMP9, are essential for ECM remodeling and angiogenesis [43,44]. MMP9 activity, specifically its active

form, was markedly elevated in PTC co-cultured with 125 and 250 MVFs, suggesting that vessel-tumor cell interactions are essential for full enzymatic activation. In contrast, MMP2 activity remained relatively constant across conditions, indicating a constitutive expression pattern by tumor cells that is not modulated by endothelial interaction. However, these findings highlight the importance of cellular crosstalk in shaping the tumor microenvironment and reinforce the angiotumoroids as a robust model for investigating tumor angiogenesis and matrix remodeling.

Neo-vasculature formation is critical for solid tumor progression, and embedding angiotumoroids in a collagen matrix provided a dynamic *in vitro* model to evaluate angiogenic potential under various MVF densities. While PTC spheroids showed no signs of neovascularization with a progressive loss of structural integrity due to peripheral cell migration, angiotumoroids with 60 and 125 MVFs displayed an enhanced and time-dependent endothelial sprouting response. This vascularization is more than observed in MVF spheroids. Notably, angiotumoroids containing 125 MVFs not only exhibited a higher expression of MMP9 but also the most robust and branched sprouting. The synergistic interaction between MVFs and PTCs was confirmed by treating MVF spheroids with PTC-conditioned medium, which significantly boosted both sprout formation and branching complexity over time, making one assume a possible communication mediated through both juxtacrine and paracrine signaling pathways. These findings identify the 125 MVF angiotumoroid condition as the potentially more physiologically representative model for *in vitro* angiogenesis, capable of recapturing some aspects of tumor-driven vascular remodeling.

Importantly, proteomic profiling of angiotumoroids revealed a unique expression signature in angiogenesis-related proteins compared to PTC spheroids, such as an increase in VEGFA, a key driver for neovascularization [45], and ECM remodeling factors, which aligns with the observed vascular development and matrix reorganization. This molecular profile mirrors the dynamic nature of *in vivo* tumor progression, where ECM degradation facilitates angiogenesis, tumor invasion, and metastasis [46]. The detection of collagen types I and IV further supports the presence of a structured ECM, which not only supports tumor cell growth but also modulates drug penetration

and immune cell infiltration [39]. Notably, the angiotumoroids exhibited upregulation of ATP-binding cassette (ABC) transporters, particularly ABCB1 (P-glycoprotein), a key mediator of drug efflux associated with multidrug resistance in cancer [47,48]. Elevated ABCB1 expression within angiotumoroids suggests the presence of localized drug resistance mechanisms, likely driven by active efflux in vascularized compartments. These findings underscore the potential of angiotumoroids not only to model tumor architecture and vascularization but also to reflect clinically relevant resistance pathways that are often absent in conventional *in vitro* systems.

Moreover, consistent with *in vivo* observations, vascularized regions within solid tumors affect drug uptake and chemotherapeutic efficacy [8,9,49]. MVFs within the angiotumoroid model significantly alter the distribution and efficacy of chemotherapeutic agents as doxorubicin, as evidenced by its different uptake and cytotoxicity. Uptake assays revealed enhanced and spatially localized drug accumulation in angiotumoroids compared to PTC spheroids. This preferential drug deposition suggests that specific regions potentially act as barriers for soluble drugs, as doxorubicin. Despite the increased drug retention, angiotumoroids exhibited reduced cytotoxicity relative to PTC spheroids after 24-hour exposure, supporting the hypothesis that in angiotumoroids, drug availability to tumor cells is modulated through sequestration mechanisms, ultimately decreasing therapeutic efficacy as demonstrated by a substantial recovery of tumor cell viability over time.

These findings strongly support the use of angiotumoroids as a versatile *in vitro* model for studying solid tumors, particularly for investigating tumor angiogenesis and tumor–vasculature crosstalk, and evaluating the delivery of anti-tumor drugs, especially for compounds designed to overcome physiological barriers in the TME. This platform is compatible with high-throughput screening, as approximately 30,000 MVFs can be obtained from just 10 grams of adipose tissue, enabling the production of around 250 angiotumoroids. Additionally, various standardized cryopreservation methods allow MVFs to be preserved efficiently, supporting large-scale collection and extended storage for future studies [50].

The angiotumoroid model, although initially established using rat-derived microvascular fragments (MVs) and tumor cells, provides a versatile framework that could be adapted to human systems. The combination of primary tumor cells obtained from patient biopsies with MVs isolated from human adipose tissue via liposuction appears technically feasible and represents a promising approach for generating patient-specific vascularized tumor constructs. Ideally, obtaining both PTCs and MVs from the same patient would be optimal, further supporting the development of personalized therapeutic approaches. However, interspecies differences in extracellular matrix composition, angiogenic signaling pathways, and immune microenvironmental factors may significantly influence the behavior and organization of the co-culture. It will therefore be essential to systematically investigate these species-specific differences to ensure the reliable adaptation and reproducibility of the model in human settings. Furthermore, the current *in vitro* configuration lacks active perfusion, limiting the physiological relevance of vascular function and metabolic exchange. Future integration of the angiotumoroid platform within microfluidic tumor-on-chip systems could provide controlled perfusion and dynamic nutrient flow, thereby improving vascular functionality, better recapitulating *in vivo* hemodynamic conditions, and ultimately enhancing the translational potential of this model for personalized oncology research.

Declarations**Ethics approval and consent to participate**

Not applicable

Consent for publication

All participants had properly consented

Availability of data and material

The datasets used and/or analysed during the current study are available from the corresponding author on reasonable request

Competing interests

The authors have no relevant financial or non-financial interests to disclose

Funding

This work has received funding from the European Union—NextGenerationEU through the Italian Ministry of University and Research under PNRR— MUR, PNRR-M4C2, ECS_00000022-Sicilian MicronanOTech Research And Innovation Center "SAMOTHRACE"—CUP: B73C22000810001.

The views and opinions expressed are those of the authors only and do not necessarily reflect those of the European Union or the European Commission. Neither the European Union nor the European Commission can be held responsible for them.

Author Contributions

ALC, FLM, and GLB designed the study. ALC, FLM, GLB, and FG performed the experiments. PC produced the recombinant collagenases. MLP and SDS performed the proteomic analysis. SC and GLB helped with data analysis. ALC analyzed data. ALC, FLM, and GLB wrote the manuscript. GG directed the study. All authors reviewed and edited the manuscript and approved the final version of the manuscript.

Acknowledgement

We are grateful to Flaviana Falci from the Antonio D'Amore group (Ri.MED Foundation) for their help with SEM analysis. We acknowledge ATeN Center—University of Palermo for the confocal microscope and the animal facility.

Bibliography

1. Giussani, M.; Triulzi, T.; Sozzi, G.; Tagliabue, E. Tumor Extracellular Matrix Remodeling: New Perspectives as a Circulating Tool in the Diagnosis and Prognosis of Solid Tumors. *Cells* **2019**, *8*, 81, doi:10.3390/cells8020081.
2. Tiwari, A.; Trivedi, R.; Lin, S.-Y. Tumor Microenvironment: Barrier or Opportunity towards Effective Cancer Therapy. *J Biomed Sci* **2022**, *29*, 83, doi:10.1186/s12929-022-00866-3.
3. Biray Avci, C.; Goker Bagca, B.; Nikanfar, M.; Takanlou, L.S.; Takanlou, M.S.; Nourazarian, A. Tumor Microenvironment and Cancer Metastasis: Molecular Mechanisms and Therapeutic Implications. *Front Pharmacol* **2024**, *15*, doi:10.3389/fphar.2024.1442888.

4. Jiang, X.; Wang, J.; Deng, X.; Xiong, F.; Zhang, S.; Gong, Z.; Li, X.; Cao, K.; Deng, H.; He, Y.; et al. The Role of Microenvironment in Tumor Angiogenesis. *Journal of Experimental & Clinical Cancer Research* **2020**, *39*, 204, doi:10.1186/s13046-020-01709-5.
5. Lugano, R.; Ramachandran, M.; Dimberg, A. Tumor Angiogenesis: Causes, Consequences, Challenges and Opportunities. *Cellular and Molecular Life Sciences* **2020**, *77*, 1745–1770, doi:10.1007/s00018-019-03351-7.
6. Al-Ostoot, F.H.; Salah, S.; Khamees, H.A.; Khanum, S.A. Tumor Angiogenesis: Current Challenges and Therapeutic Opportunities. *Cancer Treat Res Commun* **2021**, *28*, 100422, doi:10.1016/j.ctarc.2021.100422.
7. Kretschmer, M.; Rüdiger, D.; Zahler, S. Mechanical Aspects of Angiogenesis. *Cancers (Basel)* **2021**, *13*, 4987, doi:10.3390/cancers13194987.
8. Dewhirst, M.W.; Secomb, T.W. Transport of Drugs from Blood Vessels to Tumour Tissue. *Nat Rev Cancer* **2017**, *17*, 738, doi:10.1038/NRC.2017.93.
9. Primeau, A.J.; Rendon, A.; Hedley, D.; Lilge, L.; Tannock, I.F. The Distribution of the Anticancer Drug Doxorubicin in Relation to Blood Vessels in Solid Tumors. *Clinical Cancer Research* **2005**, *11*, 8782–8788, doi:10.1158/1078-0432.CCR-05-1664.
10. Urzi, O.; Gasparro, R.; Costanzo, E.; De Luca, A.; Giavaresi, G.; Fontana, S.; Alessandro, R. Three-Dimensional Cell Cultures: The Bridge between In Vitro and In Vivo Models. *Int J Mol Sci* **2023**, *24*, 12046, doi:10.3390/ijms241512046.
11. Froehlich, K.; Haeger, J.-D.; Heger, J.; Pastuschek, J.; Photini, S.M.; Yan, Y.; Lupp, A.; Pfarrer, C.; Mrowka, R.; Schleußner, E.; et al. Generation of Multicellular Breast Cancer Tumor Spheroids: Comparison of Different Protocols. *J Mammary Gland Biol Neoplasia* **2016**, *21*, 89–98, doi:10.1007/s10911-016-9359-2.
12. Lo Cicero, A.; Campora, S.; Lo Buglio, G.; Ciná, P.; Lo Pinto, M.; Scilabra, S.D.; Ghersi, G. Enhancing Therapeutic Efficacy through Degradation of Endogenous Extracellular Matrix in Primary Breast Tumor Spheroids. *FEBS Journal* **2025**, doi:10.1111/febs.70069.
13. Aggarwal, V.; Miranda, O.; Johnston, P.A.; Sant, S. Three Dimensional Engineered Models to Study Hypoxia Biology in Breast Cancer. *Cancer Lett* **2020**, *490*, 124, doi:10.1016/J.CANLET.2020.05.030.
14. Close, D.A.; Johnston, P.A. Detection and Impact of Hypoxic Regions in Multicellular Tumor Spheroid Cultures Formed by Head and Neck Squamous Cell Carcinoma Cells Lines. *SLAS Discovery* **2022**, *27*, 39–54, doi:10.1016/J.SLASD.2021.10.008.
15. Arora, L.; Kalia, M.; Roy, S.; Pal, D. Assessment of Mitochondrial Health in Cancer-Associated Fibroblasts Isolated from 3D Multicellular Lung Tumor Spheroids. *Journal of Visualized Experiments* **2022**, doi:10.3791/64315-v.
16. Parashar, D.; Geethadevi, A.; Mittal, S.; McAlarnen, L.; George, J.; Kadamberi, I.; Gupta, P.; Uyar, D.; Hopp, E.; Drendel, H.; et al. Patient-Derived Ovarian Cancer Spheroids Rely on PI3K-AKT Signaling Addiction for Cancer Stemness and Chemoresistance. *Cancers (Basel)* **2022**, *14*, 958, doi:10.3390/cancers14040958.
17. Yang, Y.; Li, S.; Sun, Y.; Zhang, D.; Zhao, Z.; Liu, L. Reversing Platinum Resistance in Ovarian Cancer Multicellular Spheroids by Targeting Bcl-2. *Onco Targets Ther* **2019**, *Volume 12*, 897–906, doi:10.2147/OTT.S187015.
18. Song, Y.; Kim, J.-S.; Kim, S.-H.; Park, Y.K.; Yu, E.; Kim, K.-H.; Seo, E.-J.; Oh, H.-B.; Lee, H.C.; Kim, K.M.; et al. Patient-Derived Multicellular Tumor Spheroids towards Optimized Treatment for Patients with Hepatocellular Carcinoma. *Journal of Experimental & Clinical Cancer Research* **2018**, *37*, 109, doi:10.1186/s13046-018-0752-0.
19. Yoshida, T.; Sopko, N.A.; Kates, M.; Liu, X.; Joice, G.; McConkey, D.J.; Bivalacqua, T.J. Three-Dimensional Organoid Culture Reveals Involvement of Wnt/ β -Catenin Pathway in Proliferation of Bladder Cancer Cells. *Oncotarget* **2018**, *9*, 11060–11070, doi:10.18632/oncotarget.24308.

20. Gottfried, E.; Rogenhofer, S.; Waibel, H.; Kunz-Schughart, L.A.; Reichle, A.; Wehrstein, M.; Peuker, A.; Peter, K.; Hartmannsgruber, G.; Andreesen, R.; et al. Pioglitazone Modulates Tumor Cell Metabolism and Proliferation in Multicellular Tumor Spheroids. *Cancer Chemother Pharmacol* **2011**, *67*, 117–126, doi:10.1007/s00280-010-1294-0.
21. Hawinkels, L.J.A.C.; Zuidwijk, K.; Verspaget, H.W.; de Jonge-Muller, E.S.M.; Duijn, W. van; Ferreira, V.; Fontijn, R.D.; David, G.; Hommes, D.W.; Lamers, C.B.H.W.; et al. VEGF Release by MMP-9 Mediated Heparan Sulphate Cleavage Induces Colorectal Cancer Angiogenesis. *Eur J Cancer* **2008**, *44*, 1904–1913, doi:10.1016/j.ejca.2008.06.031.
22. Heo, D.N.; Hospodiuk, M.; Ozbolat, I.T. Synergistic Interplay between Human MSCs and HUVECs in 3D Spheroids Laden in Collagen/Fibrin Hydrogels for Bone Tissue Engineering. *Acta Biomater* **2019**, *95*, 348–356, doi:10.1016/j.actbio.2019.02.046.
23. Shoval, H.; Karsch-Bluman, A.; Brill-Karniely, Y.; Stern, T.; Zamir, G.; Hubert, A.; Benny, O. Tumor Cells and Their Crosstalk with Endothelial Cells in 3D Spheroids. *Scientific Reports 2017 7:1* **2017**, *7*, 1–11, doi:10.1038/s41598-017-10699-y.
24. Strobel, H.A.; Moss, S.M.; Hoying, J.B. Isolated Fragments of Intact Microvessels: Tissue Vascularization, Modeling, and Therapeutics. *Microcirculation* **2024**, *31*, doi:10.1111/micc.12852.
25. Laschke, M.W.; Menger, M.D. Adipose Tissue-Derived Microvascular Fragments: Natural Vascularization Units for Regenerative Medicine. *Trends Biotechnol* **2015**, *33*, 442–448, doi:10.1016/j.tibtech.2015.06.001.
26. Laschke, M.W.; Später, T.; Menger, M.D. Microvascular Fragments: More Than Just Natural Vascularization Units. *Trends Biotechnol* **2021**, *39*, 24–33, doi:10.1016/j.tibtech.2020.06.001.
27. Shepherd, B.R.; Chen, H.Y.S.; Smith, C.M.; Gruionu, G.; Williams, S.K.; Hoying, J.B. Rapid Perfusion and Network Remodeling in a Microvascular Construct After Implantation. *Arterioscler Thromb Vasc Biol* **2004**, *24*, 898–904, doi:10.1161/01.ATV.0000124103.86943.1e.
28. Hoying, J.B.; Boswell, C.A.; Williams, S.K. Angiogenic Potential of Microvessel Fragments Established in Three-Dimensional Collagen Gels. *In Vitro Cell Dev Biol Anim* **1996**, *32*, 409–419, doi:10.1007/BF02723003.
29. Nalbach, L.; Müller, D.; Wrublewsky, S.; Metzger, W.; Menger, M.D.; Laschke, M.W.; Ampofo, E. Microvascular Fragment Spheroids: Three-Dimensional Vascularization Units for Tissue Engineering and Regeneration. *J Tissue Eng* **2021**, *12*, doi:10.1177/20417314211035593.
30. Strobel, H.A.; Gerton, T.; Hoying, J.B. Vascularized Adipocyte Organoid Model Using Isolated Human Microvessel Fragments. *Biofabrication* **2021**, *13*, 035022, doi:10.1088/1758-5090/abe187.
31. Quan, Y.; Zhang, Y.; Li, J.; Lu, F.; Cai, J. Transplantation of in Vitro Prefabricated Adipose Organoids Attenuates Skin Fibrosis by Restoring Subcutaneous Fat and Inducing Dermal Adipogenesis. *The FASEB Journal* **2023**, *37*, doi:10.1096/fj.202202117R.
32. Wrublewsky, S.; Schultz, J.; Ammo, T.; Bickelmann, C.; Metzger, W.; Später, T.; Pohlemann, T.; Menger, M.D.; Laschke, M.W. Biofabrication of Prevascularized Spheroids for Bone Tissue Engineering by Fusion of Microvascular Fragments with Osteoblasts. *Front Bioeng Biotechnol* **2024**, *12*, doi:10.3389/fbioe.2024.1436519.
33. Salamone, M.; Rigogliuso, S.; Nicosia, A.; Campora, S.; Bruno, C.M.; Ghersi, G. 3D Collagen Hydrogel Promotes In Vitro Langerhans Islets Vascularization through Ad-MVFs Angiogenic Activity. *Biomedicines* **2021**, *9*, 739, doi:10.3390/biomedicines9070739.
34. Burkel, B.; Morris, B.A.; Ponik, S.M.; Riching, K.M.; Eliceiri, K.W.; Keely, P.J. Preparation of 3D Collagen Gels and Microchannels for the Study of 3D Interactions & In Vivo & In Vivo & In Vivo. *Journal of Visualized Experiments* **2016**, doi:10.3791/53989.

35. Wiśniewski, J.R.; Zougman, A.; Nagaraj, N.; Mann, M. Universal Sample Preparation Method for Proteome Analysis. *Nat Methods* **2009**, *6*, 359–362, doi:10.1038/NMETH.1322.
36. Rappsilber, J.; Ishihama, Y.; Mann, M. Stop and Go Extraction Tips for Matrix-Assisted Laser Desorption/Ionization, Nanoelectrospray, and LC/MS Sample Pretreatment in Proteomics. *Anal Chem* **2003**, *75*, 663–670, doi:10.1021/AC026117I.
37. Rabienezhad Ganji, N.; Urzi, O.; Tinnirello, V.; Costanzo, E.; Polito, G.; Palumbo Piccionello, A.; Manno, M.; Raccosta, S.; Gallo, A.; Lo Pinto, M.; et al. Proof-of-Concept Study on the Use of Tangerine-Derived Nanovesicles as siRNA Delivery Vehicles toward Colorectal Cancer Cell Line SW480. *Int J Mol Sci* **2024**, *25*, 546, doi:10.3390/IJMS25010546/S1.
38. Robey, R.W.; Pluchino, K.M.; Hall, M.D.; Fojo, A.T.; Bates, S.E.; Gottesman, M.M. Revisiting the Role of ABC Transporters in Multidrug-Resistant Cancer. *Nature Reviews Cancer* **2018**, *18*, 452–464, doi:10.1038/s41568-018-0005-8.
39. Lo Buglio, G.; Lo Cicero, A.; Campora, S.; Ghersi, G. The Multifaced Role of Collagen in Cancer Development and Progression. *Int J Mol Sci* **2024**, *25*.
40. Ascheid, D.; Baumann, M.; Pinnecker, J.; Friedrich, M.; Szi-Marton, D.; Medved, C.; Bundalo, M.; Ortmann, V.; Öztürk, A.; Nandigama, R.; et al. A Vascularized Breast Cancer Spheroid Platform for the Ranked Evaluation of Tumor Microenvironment-Targeted Drugs by Light Sheet Fluorescence Microscopy. *Nature Communications* **2024**, *15*, 1–23, doi:10.1038/s41467-024-48010-z.
41. Moss, S.M.; Gerton, T.; Strobel, H.A.; Hoying, J.B. Isolated Human Adipose Microvessels Retain Native Microvessel Structure and Recapitulate Sprouting Angiogenesis. *Angiogenesis* **2025**, *28*, 1–13, doi:10.1007/S10456-025-09972-W/FIGURES/4.
42. Lertkiatmongkol, P.; Liao, D.; Mei, H.; Hu, Y.; Newman, P.J. Endothelial Functions of PECAM-1 (CD31). *Curr Opin Hematol* **2016**, *23*, 253, doi:10.1097/MOH.0000000000000239.
43. Quintero-Fabián, S.; Arreola, R.; Becerril-Villanueva, E.; Torres-Romero, J.C.; Arana-Argáez, V.; Lara-Riegos, J.; Ramírez-Camacho, M.A.; Alvarez-Sánchez, M.E. Role of Matrix Metalloproteinases in Angiogenesis and Cancer. *Front Oncol* **2019**, *9*, 1370, doi:10.3389/FONC.2019.01370.
44. Bergers, G.; Brekken, R.; McMahon, G.; Vu, T.H.; Itoh, T.; Tamaki, K.; Tanzawa, K.; Thorpe, P.; Itohara, S.; Werb, Z.; et al. Matrix Metalloproteinase-9 Triggers the Angiogenic Switch during Carcinogenesis. *Nat Cell Biol* **2000**, *2*, 737–744, doi:10.1038/35036374.
45. Lee, C.; Kim, M.J.; Kumar, A.; Lee, H.W.; Yang, Y.; Kim, Y. Vascular Endothelial Growth Factor Signaling in Health and Disease: From Molecular Mechanisms to Therapeutic Perspectives. *Signal Transduction and Targeted Therapy* **2025**, *10*, 1–40, doi:10.1038/s41392-025-02249-0.
46. Zhang, M.; Zhang, B. Extracellular Matrix Stiffness: Mechanisms in Tumor Progression and Therapeutic Potential in Cancer. *Experimental Hematology & Oncology* **2025**, *14*, 1–34, doi:10.1186/S40164-025-00647-2.
47. Duvivier, L.; Gerard, L.; Diaz, A.; Gillet, J.P. Linking ABC Transporters to the Hallmarks of Cancer. *Trends Cancer* **2024**, *10*, 124–134, doi:10.1016/J.TRECAN.2023.09.013/ASSET/03262B91-2C4C-4B34-A3C8-2F98046823D9/MAIN.ASSETS/GR1.JPG.
48. Morimoto, M.; Maishi, N.; Hida, K. Acquisition of Drug Resistance in Endothelial Cells by Tumor-Derived Extracellular Vesicles and Cancer Progression. *Cancer Drug Resist* **2024**, *7*, doi:10.20517/CDR.2023.121.
49. Trédan, O.; Galmarini, C.M.; Patel, K.; Tannock, I.F. Drug Resistance and the Solid Tumor Microenvironment. *JNCI: Journal of the National Cancer Institute* **2007**, *99*, 1441–1454, doi:10.1093/JNCI/DJM135.

50. Laschke, M.W.; Karschnia, P.; Scheuer, C.; Heß, A.; Metzger, W.; Menger, M.D. Effects of Cryopreservation on Adipose Tissue-Derived Microvascular Fragments. *J Tissue Eng Regen Med* **2018**, *12*, 1020–1030, doi:10.1002/TERM.2591.

ARTICLE IN PRESS